Structure, Volume *24*

Supplemental Information

Structural Basis of Interfacial Flexibility in Fibrin Oligomers

Artem Zhmurov, Anna D. Protopopova, Rustem I. Litvinov, Pavel Zhukov, Alexander R. Mukhitov, John W. Weisel, and Valeri Barsegov

SUPPLEMENTAL TABLES

Table S1. Related to Figure 2. Crystal structures of human fibrinogen, fibrin, and their fragments from PDB used in the reconstruction of fibrin oligomers.

PDB codes	Structures	References
Fibrinogen		
3GHG	Human fibrinogen co-crystallized with GPRP and GHRP	Kollman et al., 2009
D-dimer fragments from crosslinked fibrin		
1FZB	Crosslinked double D fragment	Spraggon et al., 1997
1FZC	Fragment double-D from human fibrin with bound ligands	Everse et al., 1998
1FZE	Fragment double-D from human fibrin	Everse et al., 1999
1FZF	Fragment double-D from human fibrin with GHRP	Everse et al., 1999
1N86	Human D-dimer from cross-linked fibrin with GPR and GHRPLDK	Yang et al., 2002
1N8E	Fragment double-D from human fibrin	Yang et al., 2002
2HLO	Fragment D-dimer from human fibrin with G-hydroxyP-RP	no reference
2HOD	Fragment D-dimer from human fibrin with G-hydroxyP-RP	no reference
2HPC	Fragment D-dimer from human fibrin with GPRP	no reference
2Q9I	D-dimer from human fibrin with MHRPY	Doolittle and Pandi, 2007
2Z4E	D-dimer from human fibrin with GHRPY	Pandi et al., 2009
3H32	D-dimer from human fibrin with GHRPY	Pandi et al., 2009
Fragments D (D-D interactions in a crystal as a result of molecular packing)		
1FZG	Fragment D from human fibrinogen with GHRP	Everse et al., 1999
2H43	Fragment D co-complexed with AHRP	Doolittle et al., 2006
2FFD	Fibrinogen fragment D with GPRVVE	Betts et al., 2006
3BVH	Recombinant γD364A fibrinogen fragment D with GPRP	Bowley et al., 2008
3E1I	BβD432A variant fibrinogen fragment D with GHRP	Bowley and Lord, 2009
2OYH	Fragment D of γD298,301A fibrinogen variant with GHRP	Kostelansky et al., 2007
2OYI	Fragment D of γD298,301A fibrinogen variant with GHRP	Kostelansky et al., 2007
1LT9	Recombinant human fibrinogen fragment D	Kostelansky et al., 2002
1LTJ	Recombinant human fibrinogen fragment D with GPRP and GHRP	Kostelansky et al., 2002
1FZA	Fibrinogen fragment D	Spraggon et al., 1997
1RE3	Fragment D of BβD398A fibrinogen variant with GHRP	Kostelansky et al., 2004
1RE4	Fragment D of BβD398A variant fibrinogen	Kostelansky et al., 2004
1RF1	Fragment D of γE132A fibrinogen variant with GHRP	Kostelansky et al., 2004
1RF0	Fragment D of γE132A fibrinogen variant	Kostelansky et al., 2004

Table S2. Related to Figure 5. Naturally occurring fibrinogen mutations and their relation to the inter-residue contacts in the D:E:D interface: Binary contacts between amino acid residues in the D-D structures and in the central E region resolved by the X-ray crystallography. Only residues with known natural fibrinogen variants containing corresponding point mutations are listed. The molecular characteristics of fibrinogen variants are taken from GEHT database (Hanss and Biot, 2001).

Residue in the D:D interface identified in this study	Fibrinogen variants with mutated amino acids shown in the left column	Corresponding reacting partner residues in the E region
γAsp318	→Tyr (Bastia)	BβLys53, BβArg57
	→Gly (Giessen IV)	
	→Val (Caen)	
γAsn319	→Lys	BβArg57
	→deleted (Hannover)	
γAsp320	→deleted (Des Moines)	BβArg57
	→Gly (Chinese)	
γAsn319-Asp320	→deleted (Vlissingen, Frankfurt IV, Otsu)	AαArg23, AαLys29, BβArg57
γPhe322	→Cys (Villeurbanne)	AαVal21-Ser27, AαLys29, BβGlu56-Lys58, BβPro60
γAsn325	→Ile (Krakow)	AαVal21-Arg23, BβLys53, BβVal56-Lys58, BβPro70-Asp71, γGln49
γCys326	→Ser (Cordoba, Hannover XIII)	AαVal21, BβGlu56
	→Tyr (Suhl, Frostburg)	
γAla327	→Thr (Tokyo V)	γAsp37-Lys38
γGln329	→Arg (Nagoya)	AαVal21-Arg23, AαLeu54, AαGlu57, AαPhe62, AαArg65, BβLys54, BβGlu56-Lys58, γGln49, γGln33, γAsp37
γAsp330	→Tyr (Kyoto III)	AαArg65, γAsp37, γGln41
	→Val (Ales, Milano)	
γAsn337	→Lys (Bern)	AαGlu22-Gln25
γGln350	not documented	AαLys68-Leu69, AαLeu73
γGly351	→14 aa (Paris)	AαLys68
	→Ser (Praha, Leipzig II)	
γGly352	→Cys (Ilam)	AαLys68
γThr353	→Pro (Ilam)	AαLys68
γAsn361	→Lys (Poissy II)	AαVal21-Arg23, BβVal56-Arg57
γTyr363	→Asn (Praha III)	AαVal21-Arg23, BβVal56-Arg57
γAsp364	→His (Matsumoto)	AαVal21
	→Val (Melun)	
γArg375	→Gly (Osaka V)	AαVal21
	→Trp (Aguadilla, Geneva, Italian, San Diego, Japanese)	

SUPPLEMENTAL FIGURES

Figure S1. Complementary to Figure 2. Flexibility of the D-dimers
(A and B) Comparison of D-D interfacial contacts found in naturally formed D-dimers (A) with those reported as crystal contacts (B). Both sets have similar variations in the bending angle formed by two fibrin(ogen) monomers. Two clusters of structures (named Clusters 1 and 2 in the Main Text) have been identified: Cluster 1 contains intermolecular contacts from the following PDB structures: 1N86, 2HOD, 2HPC, 3H32, and 3BVH. Cluster 2 contains contacts from the following PDB structures: 1FZB, 1FZE, 1FZF, 1N8E, 2HLO, 2Q9I, 2Z4E, 1FZG, 2H43, 3E1I, 2OYH, 2OYI, 1LT9, 1LTJ, 1FZA, 1RE3, 1RE4, 1RF1, and 1RF0. The average structures for Clusters 1 and 2 marked bold were used in our computational reconstruction.
(C) RMSF values for residues in the γ1 nodule relative to the γ2 nodule and vice versa.
(D and E) Results of Normal Mode analysis for two head-to-tail connected fibrin monomers performed with the elNemo web-interface (Suhre and Sanejouand, 2004-1; Suhre and Sanejouand, 2004-2). The equilibrium structure is shown ghosted, and the structures exemplifying the normal modes are in color (directions of motion are shown by the black arrows). Modes 7 (D) and 8 (E) represent the bending motion of fibrin dimer around the identified hinge region in the D-D interface (see Main Text).

Figure S2. Related to Figure 3. Geometric constrains associated with knob 'A' binding to hole 'a' in the D-E-D complex
(A) Depicted are the β- and γ-nodules of two abutted fibrin monomers forming the upper strand and the E region in the lower strand. The GPRV motifs comprising the knob 'A'-containing N-terminal part of the α chain (knob 'A'-mimetic peptide GPRP) are inserted into holes 'a' of the γ-nodules of two adjacent fibrin monomers. The first resolved residue in the α chain is αAla27 in the E region. In the case of A-a interaction, the distance between position of αVal20 of the GPRV motif (corresponding to position of Pro4 in the peptide GPRP) and position of αAla27 in the E region cannot exceed the contour length of the 6-mer peptide connecting the C_α atoms of these residues. This is a 6-residue-long stretch with a contour length of ~26-27Å.
(B) All 8 constraints (dashed red curves), which have to be simultaneously satisfied in reconstruction of $FO_{2/3}$.

Figure S3. Related to Figure 4. AFM images and atomic models of double-stranded fibrin oligomers
(A-D) The AFM images of short fibrin oligomers $FO_{1/2}$ (A), $FO_{2/2}$ (B), $FO_{2/3}$ (B) and longer oligomers $FO_{4/4}$ and $FO_{6/6}$ (B). Shown are the raw AFM images (top panels), AFM images with approximate positions of D and E regions (middle panels), and AFM images with superimposed *in silico* structures (bottom panels).
(E) The dynamics of D-E distances from 20 Monte Carlo docking runs (final stage of structural relaxation for each run is magnified in *the inset*). The grey area on the inset indicates the experimental range of D-E distances from AFM images.

Figure S4. Related to Figure 5. Structures of knob 'B' bound to complementary hole 'b'
(A and B) Contiguous parts of the β-nodule with Ca^{2+} and disulfide bonds, portions of the α, β and γ chains forming the triple-helical coiled coil, and carbohydrates. Panels (A) and (B) represent two possible ways for the knob 'B' to bind to the hole 'b' by routing around the carbohydrate chain, which is linked to residue βAsn364 in the β-nodule. In panel (A), knob 'B' – part of the Nβ region (Medved and Weisel, 2009), directly approaches hole 'b' that is not obstructed by the carbohydrate chain. In panel (B), knob 'B' winds around the carbohydrate and approaches hole 'b' through the space between the carbohydrate and the coiled-coil region. The average potential energies of these two conformations of the B-b knob-hole complex are within their standard deviations, implying that both binding scenarios are possible. The atomic models are based on the MD simulations of atomic structures created using crystallographic data from the structure 3GHG of fibrinogen and the structure 1N86 of D:D interface (Table S1; see Data S3).

Figure S5. Crosslinking of fibrinogen and fibrin oligomers. SDS-PAGE in reducing conditions showing the subunit composition of fibrinogen (Fg) and fibrin (Fn) oligomers before, during, and after incubation with pre-activated factor XIIIa (see Methods).
(A) Lanes (from left to right) show control untreated fibrinogen without factor XIIIa and the crosslinking products after incubation of fibrinogen with factor XIIIa for 40 sec, 3 min, 15 min, 30 min, and 60 min. Horizontal arrows indicate the bands corresponding to the γ-dimers as well as the Aα, Bβ, and γ subunits. The dashed vertical line between the 30-min and 60-min lanes reflects the fact that an uninformative auxiliary lane with lower protein loading has been spliced from the original gel.

(B) Lanes show fibrin oligomers formed by treating fibrinogen with thrombin in the absence (left lane) and presence of factor XIIIa activity. The γ-dimer band indicates covalent intermolecular crosslinking.
(C and D) Quantitative analysis of the gels shown in (A) and (B), respectively. SDS-PAGE of fibrinogen (A and C) shows only partial γ-γ crosslinking because the sample contained a mixture of uncrosslinked fibrinogen monomers and short soluble crosslinked fibrinogen oligomers, while fully crosslinked insoluble fibrinogen polymers have been removed. SDS-PAGE of fibrin (B and D) shows incomplete γ-γ crosslinking because of a very low fibrin(ogen) concentration (3 μg/ml) and a relatively short time of incubation with factor XIIIa (15-20 min).

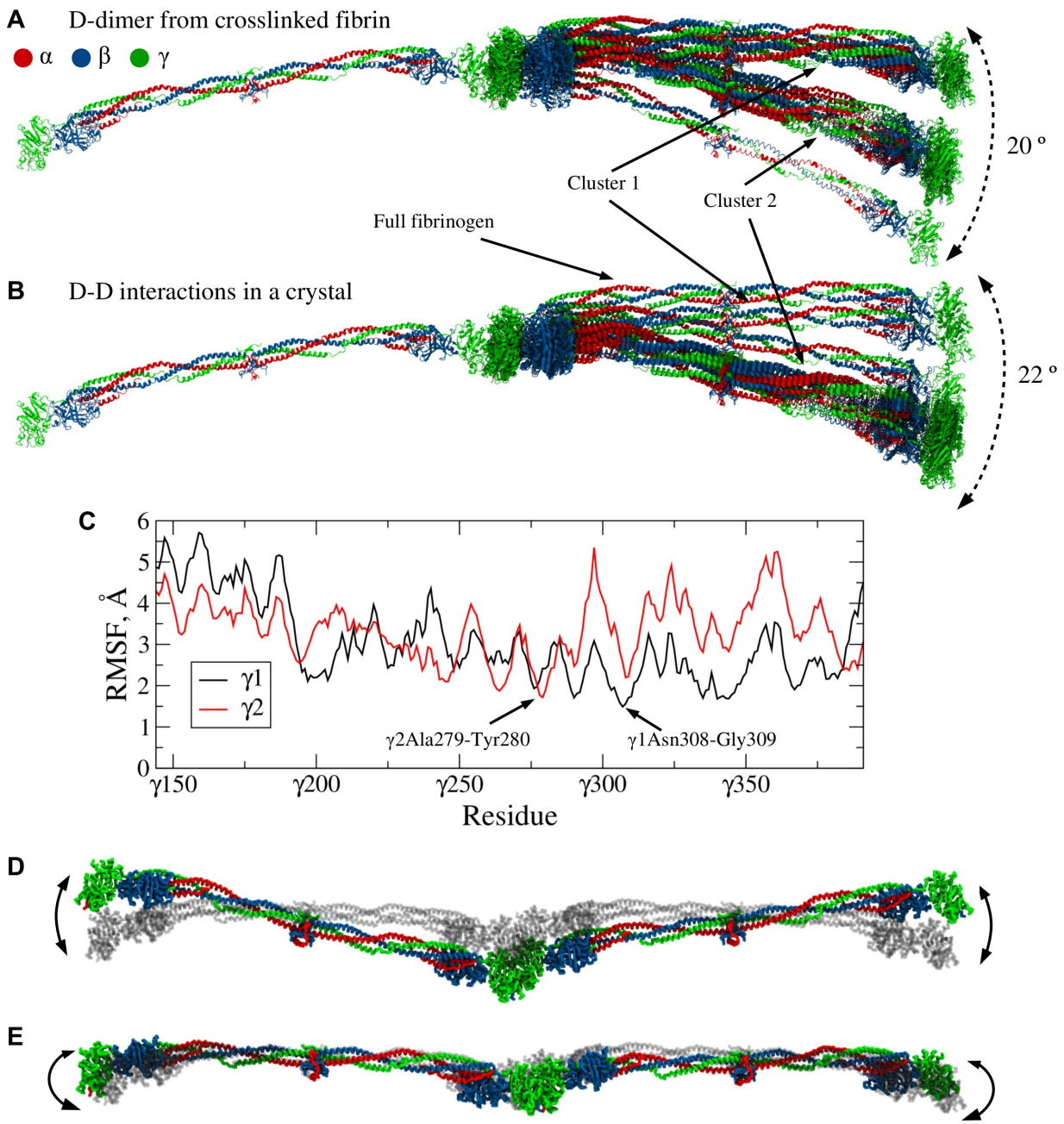
A
D-dimer from crosslinked fibrin
α
β
γ
20 °
Cluster 1
Cluster 2
Full fibrinogen
B
D-D interactions in a crystal
22 °
C
RMSF, Å
γ1
γ2
γ2Ala279-Tyr280
γ1Asn308-Gly309
γ150
γ200
γ250
γ300
γ350
Residue
D
E

Figure S1

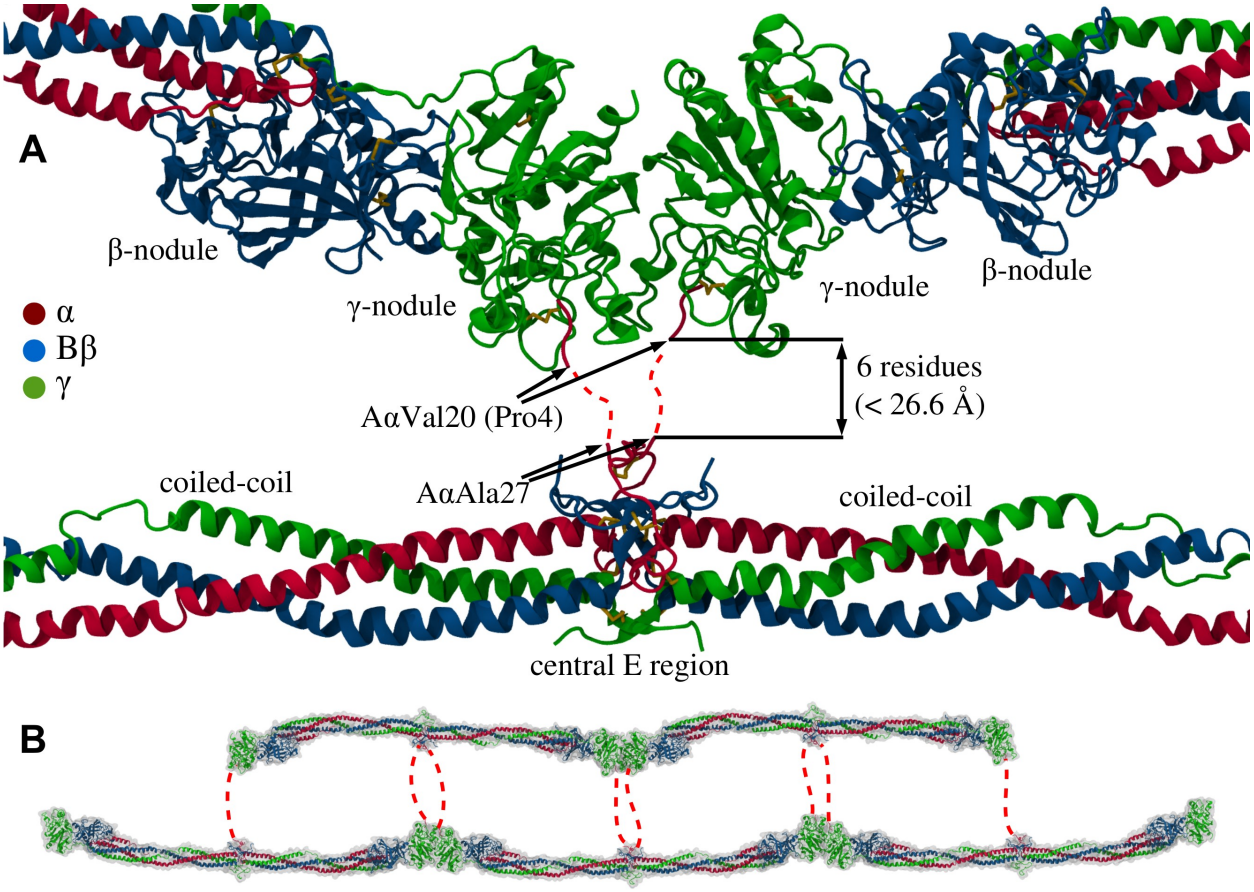
A
β-nodule
γ-nodule
γ-nodule
β-nodule
α
Bβ
γ
6 residues
(< 26.6 Å)
AαVal20 (Pro4)
AαAla27
coiled-coil
coiled-coil
central E region
B

Figure S2

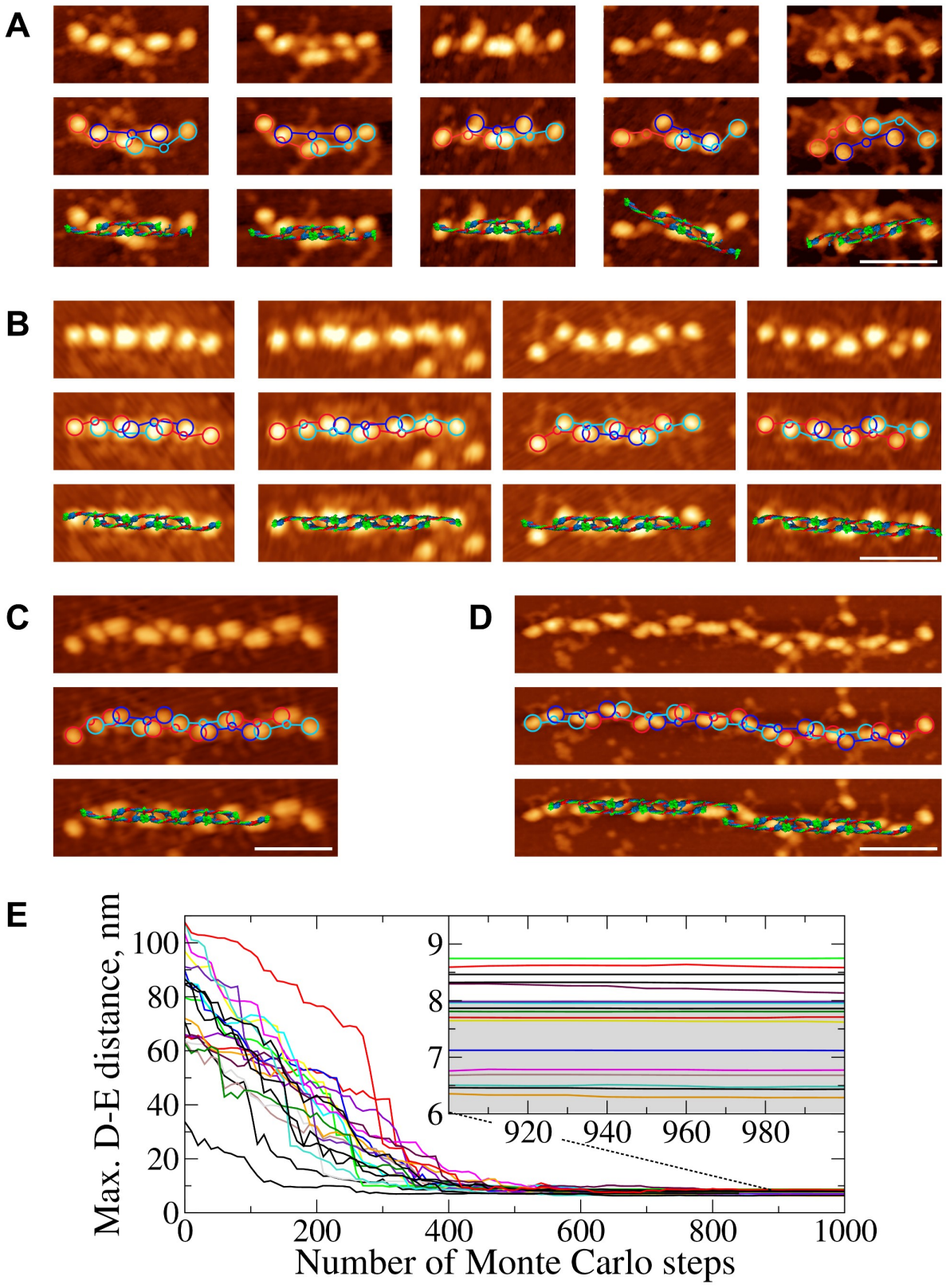
A
B
C
D
E
Max. D-E distance, nm
Number of Monte Carlo steps
0
20
40
60
80
100
0
200
400
600
800
1000
6
7
8
9
920
940
960
980

Figure S3

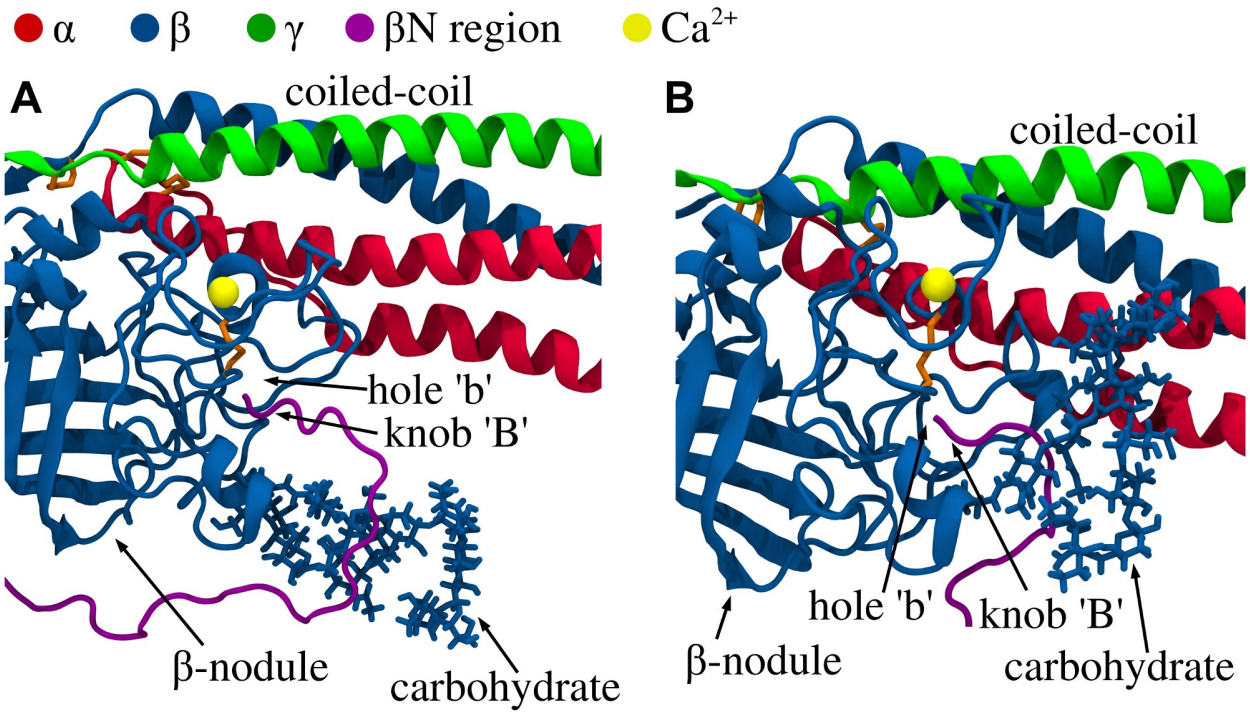
α
β
γ
βN region
Ca2+
A
coiled-coil
hole 'b'
knob 'B'
β-nodule
carbohydrate
B
coiled-coil
hole 'b'
knob 'B'
β-nodule
carbohydrate

Figure S4

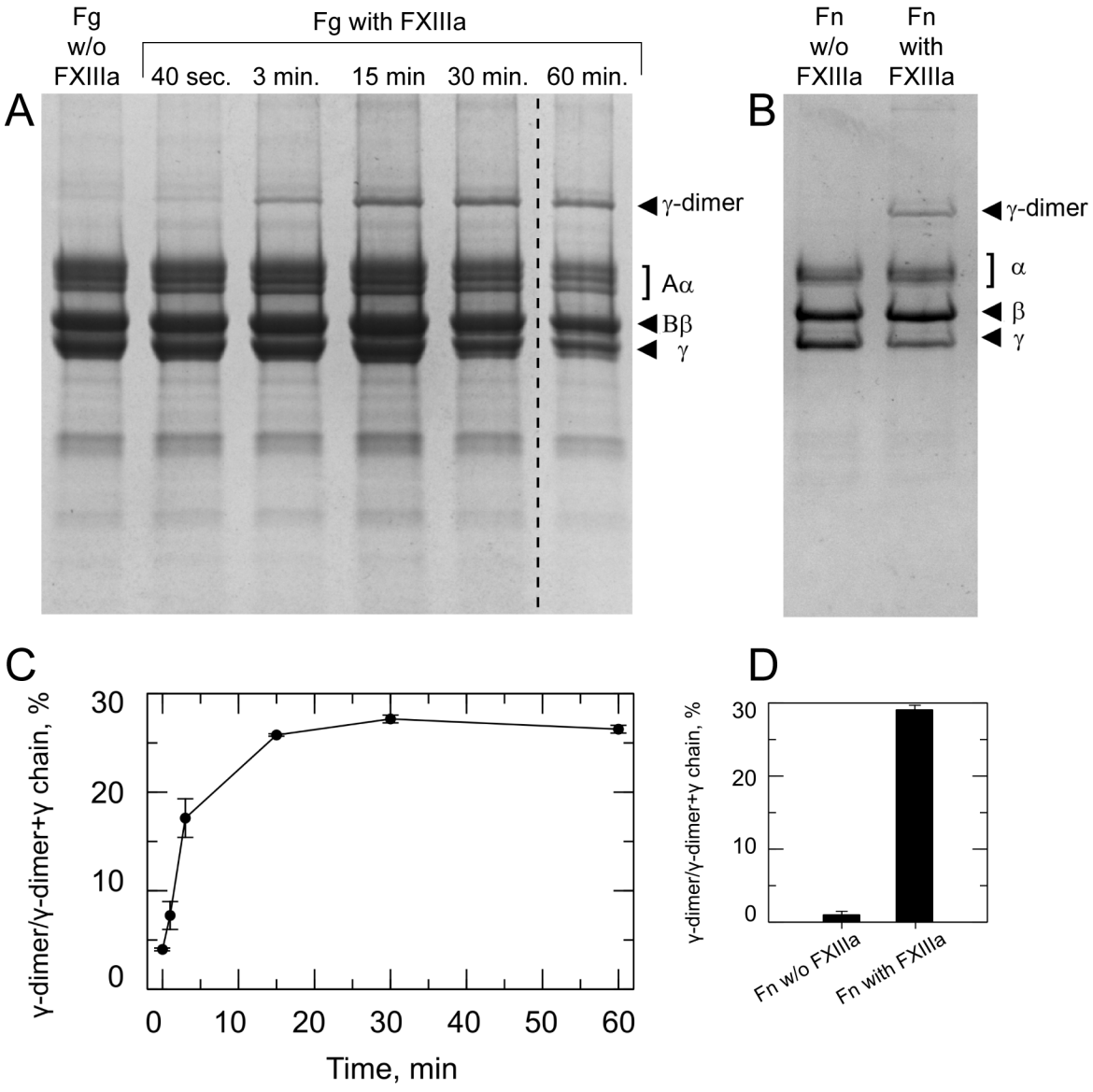
Fg w/o FXIIIa
Fg with FXIIIa
40 sec.
3 min.
15 min
30 min.
60 min.
A
γ-dimer
Aα
Bβ
γ
Fn w/o FXIIIa
Fn with FXIIIa
B
γ-dimer
α
β
γ
C
γ-dimer/γ-dimer+γ chain, %
Time, min
D
γ-dimer/γ-dimer+γ chain, %
Fn w/o FXIIIa
Fn with FXIIIa

Figure S5

SUPPLEMENTAL STRUCTURES

Data S1 related to Figure 2D: Structure alignment of two fibrin monomers obtained from the crystal structures of human fibrinogen. Positions of one monomer relative to the other are combined into 28 molecular models in one PDB file. The first model corresponds to the first monomer; the other 27 models correspond to the crystal structures accumulated in Table S1.

Data S2 related to Figure 3D: Structure of double-stranded fibrin oligomer $FO_{2/3}$ with γ-γ crosslinks and A-a and B-b knob-hole bonds.

Data S3 related to Figure 5: Structure of the D-E-D fragment.

SUPPLEMENTAL EXPERIMENTAL PROCEDURES

Structure alignment with Kabsch algorithm (Kabsch, 1976) is a method of finding an orthogonal transformation to overlap one set of atomic coordinates (for one structure) with another set (for another structure). Because the Kabsch algorithm minimizes the root-mean-squared deviations (RMSD) for any pair of structures, this method is widely used in the structure alignment of biomolecules. We utilized this approach to overlap two fibrinogen molecules with two fragments D at the D:D junction. We took two structures and selected the atoms to be aligned (we used the C_α atoms in the globular parts of fibrinogen molecule). The two sets of coordinates of N atoms were organized into two $3\times N$ matrices X_1 and X_2. Each row corresponded to the Cartesian coordinates of atoms from the first molecule (matrix X_1) and the second molecule (matrix X_2). Any two rows in X_1 and X_2 contained two sets of coordinates of atoms (x_1, y_1, z_1) and (x_2, y_2, z_2) to be aligned. Next, we defined the unitary rotation matrix $U = (A^TA)^{1/2}A^{-1}$, where $A = X_1^TX_2$ (superscript T denotes the matrix transpose). To overlap the second molecule with the first, we applied the transformation U to the atomic coordinates in the second molecule.

Normal mode analysis: We used the structure containing two monomers connecting head-to-tail for the Normal Mode Analysis (NMA). The analysis was done using elNemo web-interface (Suhre and Sanejouand, 2004-1; Suhre and Sanejouand, 2004-2).

Clustering analysis: To identify structural invariant among 27 available crystal structures of D-D complexes, we performed clustering analysis. As a structural characteristic of the D:D interface, we used a vector containing all distances separating the C_α-atoms of the first fragment D from the C_α-atoms of the second fragment D. We computed the vectors for all available D-D structures and then performed k-means clustering analysis of these vectors to identify the clusters with similar structures. We found that 19 structures cluster around the bent conformation, whereas 5 structures cluster around the straight conformation. We identified the structures that were the closest to the centroid structures of these clusters – the PDB structures 1FZG bent conformation) and 1N86 (straight conformation).

Steps 1-3 of computational reconstruction of short fibrin oligomers. We used the following Steps 1-3 to construct the atomic structures of double-stranded fibrin oligomer $FO_{2/3}$. *Step1: Constructing fibrinogen dimer Fg_2 and trimer Fg_3* was performed using resolved crystallographic structures (Table S1) by connecting monomers end-to-end at the D-D junction. A particular double-D structure was aligned with the full-length fibrinogen so that one of the D regions of the double-D fragment overlapped with one of the D regions of the fibrinogen molecule. We used the Kabsch algorithm (Kabsch, 1976) to align the C_α-atoms of the globular parts of the molecules. We superimposed the C_α-atoms of resolved residues Bβ197-461 in the β-nodule and γ139-411 in the γ-nodule. We repeated the above procedure used for Fg_2 to reconstruct Fg_3 (see also section "Constraints due to A-a knob-hole bonds" below). *Step 2: Initial placement of two single-stranded fibrin polymers:* We used the structures of Fg_2 and Fg_3 with straight and bent double-D fragments (PDB entries 1FZG and 1N86 respectively; Table S1). For $FO_{2/3}$, the number of constraints due to A-a knob-hole bonds is 8 (Figure S2B). We performed initial placement of Fg_2 and Fg_3 subject to these constraints using Monte-Carlo docking (Figure 3B) with a 17Å target distance between residues Val20 in knob 'A' and αAla27 in the α chain. Out of 14 structures generated starting from the straight conformation, we selected the structure with the shortest αVal20-Ala27 distances (Figure 3C) varying in a range of 7-17Å (Figure S3E). *Step 3: Incorporating unresolved residues:* In the structure obtained in Step 2, the distances between the C_α-atoms of Pro4 (GPRP) and αAla27 (central nodule) is <17Å, which allows knobs 'A' and 'B' to reach holes 'a' and 'b', respectively. We incorporated the following residues (VMD package; Humphrey et al., 1995): (i) GPRVVERHQS (with underlined knob 'A'); (ii) GHRPLDKKREEAPSLRPAPPPISGGGYRARPAKAAATQKKVER (with underlined knob 'B'); (iii) PQQ (the C-terminus of the Bβ chain); and (iv) GEGQQHHLGGAKQAGDV (the C-terminus of the γ chain with underlined γ-γ crosslinking sites). The γ-γ crosslinks were synthesized using a transglutamination patch connecting γGlu399 and γLys406 of two adjacent γ-nodules (see section "Transglutamination *in silico*" below), and the A-a and B-b bonds were formed as described below. To refine the structure, we performed energy minimization with the steepest descent algorithm (Adcock and McCammon, 2006) implemented in our package for GPU-based MD simulations with a SASA implicit solvent model (Ferrara et al., 2002; Zhmurov et al., 2012).

Constraints due to A-a knob-hole bonds: Fibrinogen molecules were co-crystallized with synthetic peptides GPRP and GHRP mimicking knobs 'A' and 'B', respectively (PDB code: 3GHG, Kollman et al., 2009). The first resolved residue in the fibrinogen's Aα chain AαAla27 is located in the E region (Figure 5 and Figure S2). The knob 'A'

(GPR) in fibrin starts from the residue αGly17. In a double-stranded oligomer, the GPR-containing N-terminal sequence of the α chain in one strand should reach the hole 'a' in another strand. We assumed that the interaction of the natural GPRV motif with hole 'a' is similar to binding of the synthetic GPRP peptide, i.e. the C_α-atoms of residues αGly17-Val20 take the positions of residues Gly1-Pro4 of GPRP in hole 'a'. Because the N-terminal Aα chain sequence AαAla1-Ala26 is unresolved (PDB code: 3GHG), this part of the fibrinogen molecule is unstructured. There are 6 amino acids connecting residue αVal20 (inserted in hole 'a' along with knob 'A') and residue αAla27 in the central E region (Figure S2). With the 3.8Å amino acid length, the contour length of a chain connecting the C_α-atoms of αVal20 and αAla27 is 7×3.8Å = 26.6Å (Figure S2). This enabled us to introduce geometric constraints for double-stranded structures – all distances between the C_α-atom of the last residue in knob 'A' (αVal20) in hole 'a' and the C_α-atom of αAla27 in the α chain should be <26.6Å (Figure S2). This helped us to determine the initial position of the two strands in double-stranded oligomers.

Monte-Carlo docking: The Monte-Carlo simulations are widely used in rigid-body protein docking (Cherfils and Janin, 1993). In these simulations, one of the molecules is constrained and the other molecule is positioned on its surface randomly using small rotations or translations moves. The rotational or translational move is accepted if a uniformly distributed random number from the unit interval [0,1] is less than the value of $p = \min\left\{1, \exp\left[-\frac{U_{n+1} - U_n}{kT}\right]\right\}$, where U_n and U_{n+1} are the interaction energies of the protein-protein complex computed at the n-th and n+1-st step. We used information about A-a knob-hole interactions between two fibrin molecules forming the complex. Because these interactions occur through flexible knobs 'A', they do not completely specify the relative position of the two monomers, and so we used the length of polypeptide chain (r) in the interaction energy function: $U = \sum_{i=1}^{I} \frac{k_s (r_i - r_0)^2}{2}$, where the summation is performed over all I specific interactions (A-a knob-hole bonds), $k_s = 10^3$ pN/nm is the spring constant, r_i is a current distance between the two ends of knob 'A', and r_0 is the target distance. We carried out Monte-Carlo simulations starting from the structure of two randomly placed fibrin monomers separated by a 20-nm distance. The length (translations) and the angle (rotations) were adjustable. Initially, we used the maximum value of 10 nm for translations and 10° for rotations. If the first 100 steps were not successful (i.e., either steric clashes occurred or Metropolis criteria was not satisfied 100 times in a row), in the next 100 steps the value of the distance/angle was cut in half, etc. These simulations were continued until the distance and angle were less than 0.001 nm and 0.001°, respectively. We used Monte-Carlo docking in Step 2 (see Figure 3A in Main Text).

Reconstructing residues missing in the crystal structures: There are amino acid residues that are reported as unresolved in the crystal structures (see Table S1). These are functionally important unstructured and flexible parts of fibrinogen molecule, its structural portions, and various structural combinations. To incorporate these residues, we synthesized the polypeptide chain using the VMD program (Humphrey et al., 1995). When adding residues one at a time, we used the values of dihedral angles φ=-180° and ψ=180° (linear conformation of polypeptide chain). These newly synthesized structures were properly translated/rotated and then covalently linked to resolved parts of the molecule. We used this in Step 3 (see Figure 3A in Main Text). The following residues were added to the crystal structure of each fibrin monomer: (1) α17-26 (knob 'A'-containing motif); (2) β15-57 (knob 'B'-containing motif); (3) β459-461 (the C-terminal part of the β chain); (4) γ1-13 (the N-terminal part of the γ chain); and (5) γ395-411 (the C-terminal part of the γ chain containing the γ-γ crosslinking site).

In silico formation of A-a and B-b knob-hole bonds: There is a 7–residue-long unstructured sequence between knob 'A' and the first resolved residue in the α chain that is missing in the PDB file. There is also a 30-residue-long missing unstructured sequence between knob 'B' and the first resolved residue in the β chain. These sequences connect GPR (in the α chain) and GHRP (in the β chain) to the central globule in the E region of an adjacent fibrin molecule. As described in Step 3, we first synthesized the polypeptide chains VVERHQS (containing knob 'A') and LDKKREEAPSLRPAPPPISGGGYRARPAKAAATQKKVER (containing knob 'B'). Next, we placed these peptides so that (1) the N-terminal part of each sequence is close to the last residue in the GPRP (GHRP) peptide and (2) the C-terminal part of each sequence is close to the first resolved residue in the corresponding portion of the central nodule. The N-terminal residues of the α and β chains containing knobs 'A' (GPRV, α17-20) and 'B' (GHRP, β15-18) were placed at the known positions of the corresponding peptides GPRP and GHRP co-crystallized with the full-length fibrinogen (PDB code 3GHG). In the GPRP peptide, the last residue is Pro4; in the knob 'A', the

corresponding residue is αVal20 (αVal20 is not a part the active portion of knob 'A'), so we reproduced positions only for the backbone atoms. After initial placement, the system was energy-minimized while the sequences GPRP and GHRP were constrained to remain in holes 'a' and 'b', respectively, to avoid the A-a and B-b knob-hole bonds dissociation.

Transglutamination in silico: The γ-γ crosslinks are covalent bonds connecting (i) residues γGlu398 or γGlu399 in the first fibrin monomer and residue γLys406 in the second monomer; and (ii) residues γGlu398 or γGlu399 in the second monomer and residue γLys406 in the first monomer. These bonds are created by an enzyme factor XIIIa through the transglutamination reaction, during which the covalent isopeptide bond is formed between the γ-acyl group of glutaminyl and the ε-amine group of lysyl. The C_γ-atom of glutamine residue was connected to the C=O-group, which was connected to the NH-group which, in turn, was connected to the C_ε-atom of lysyl. This structure resembles the backbone of two consecutive glycine residues, which allows us to describe the γ-γ crosslinks using the force field parameters for the protein backbone: CHARMM36 for proteins and carbohydrates for the MD simulations in explicit solvent; and CHARMM19 for the MD simulations in implicit water. The atoms that are released upon the transglutamination reaction (i.e. glutamine NH_2-group and two hydrogen atoms from the lysine residue) were removed. We placed sequences γ395-411 next to each other so that (a) the first unresolved residues (γGly395) were in the vicinity of the last resolved residues (γIle394) in the γ-nodules and (b) γGln398 and γLys406 in the first γ-nodule were close to γLys406 and γGln398 in the second γ-nodule. Next, we covalently linked two γGln398 with two γLys406. Hence, for each γ-γ crosslink in each double-D region we created two covalent bonds: (1) γGlu398 in the first fibrin monomer was connected with γLys406 in the second monomer and (2) γGlu398 in the second fibrin monomer was connected with γLys406 in the first monomer.

MD simulations: The all-atom MD simulations in explicit solvent (water) were performed using NAMD software (Phillips et al., 2005) with CHARMM36 force-field (MacKerell et al., 1998). The γ-E-γ construct was solvated in a 10.6 nm×6.6 nm×11.8 nm TIP3P-water box with 0.15M NaCl (pH=7; 75,035 atoms). The D-E-D construct was solvated in a 26.0 nm×13.3 nm×7.7 nm water box with 0.15M NaCl (pH=7; 243,953 atoms). We used the 12Å cutoff distance. The long range electrostatics was described with the particle mesh Ewald method. In the all-atom MD simulations in implicit water, we employed the Solvent Accessible Surface Area (SASA) model of implicit solvation, which is based on CHARMM19 force field. In the SASA model based energy calculation, the mean solvation energy $\Delta G_{solv}(r)$ is proportional to the solvent accessible surface area (SASA) of a solute molecule: $\Delta G_{solv}(r) = \sum_{i=1}^{N} \sigma_i A_i(r)$, where σ_i is the atomic solvation parameter and $A_i(r)$ is the SASA for the i-th atom (Ferrara et al., 2002).

SUPPLEMENTAL REFERENCES:

Adcock S.A., McCammon J.A. (2006). Molecular dynamics: survey of methods for simulating the activity of proteins. Chem. Rev. *106*, 1589–1615.

Betts, L., Merenbloom, B.K., and Lord, S.T. (2006). The structure of fibrinogen fragment D with 'A' knob peptide GPRVVE. J. Thromb. Haemost. *4*, 1139–1141.

Bowley, S.R., Merenbloom, B.K., Okumura, N., Betts, L., Heroux, A., Gorkun, O.V., and Lord, S.T. (2008). Polymerization-defective fibrinogen variant γD364A binds knob 'A' peptide mimic. Biochemistry 47, 8607–8613.

Cherfils J., Janin J. (1993) Protein docking algorithms: simulating molecular recognition. Curr. Opin. Struct. Biol. *3*, 265–269.

Doolittle, R.F., Chen, A., and Pandi, L. (2006). Differences in binding specificity for the homologous γ- and β-chain 'holes' on fibrinogen: exclusive binding of Ala-His-Arg-Pro-amide by the β-chain hole. Biochemistry *45*, 13962–13969.

Doolittle, R.F., and Pandi. L. (2007). Probing the beta-chain hole of fibrinogen with synthetic peptides that differ at their amino termini. Biochemistry *46*, 10033–10038.

Everse, S.J., Spraggon, G., Veerapandian, L., and Doolittle, R.F. (1999). Conformational changes in fragments D and double-D from human fibrin(ogen) upon binding the peptide ligand Gly-His-Arg-Pro-amide. Biochemistry *38*, 2941–2946.

Ferrara, P., Apostolakis, J. and Caflisch, A. (2002). Evaluation of a fast implicit solvent model for molecular dynamics simulations. Proteins *46*, 24–33.

Humphrey, W., Dalke, A. and Schulten, K. (1995). VMD - Visual Molecular Dynamics. J. Molec. Graphics *14*, 33–38.

Kabsch, W. (1976). A solution for the best rotation to relate two sets of vectors. Acta Crystallographica *32*, 922–923.

Kostelansky, M.S., Bolliger-Stucki, B., Betts, L., Gorkun, O.V., and Lord, S.T. (2004). BβGlu397 and BβAsp398 but not BβAsp432 are required for 'B:b' interactions. Biochemistry *43*, 2465–2474.

Kostelansky, M.S., Lounes, K.C., Ping, L.F., Dickerson, S.K., Gorkun, O.V., Lord, S.T. (2007). Probing the γ2 calcium-binding site: studies with γD298,301A fibrinogen reveal changes in the γ294-301 Loop that alter the integrity of the 'a' polymerization site. Biochemistry *46*, 5114–5123.

MacKerell, Jr., A.D., et. al. (1998) All-atom empirical potential for molecular modeling and dynamics studies of proteins. J. Phys. Chem. B *102*, 3586–3616.

Medved, L., and Weisel, J. W. (2009). Recommendations for nomenclature on fibrinogen and fibrin. J. Thromb. Haemost. *7*, 355-359.

Pandi, L., Kollman, J.M., Lopez-Lira, F., Burrows, J.M., Riley, M., and Doolittle, R.F. (2009). Two families of synthetic peptides that enhance fibrin turbidity and delay fibrinolysis by different mechanisms. Biochemistry *48*, 7201–7208.

Phillips, J.C., Braun, R., Wang, W., Gumbart, J., Tajkhorshid, E., Villa, E., Chipot, C., Skeel, R.D., Kalé, L. and Schulten, K. (2005) Scalable molecular dynamics with NAMD. J. Comput. Chem. *26*, 1781–1802.

Spraggon, G., Everse, S.J., and Doolittle, R.F. (1997). Crystal structures of fragment D from human fibrinogen and its crosslinked counterpart from fibrin. Nature *389*, 455–462.

Suhre, K., Sanejouand, Y. H. (2004). ElNemo: a normal mode web server for protein movement analysis and the generation of templates for molecular replacement. *Nucleic Acids Res. 32*(suppl 2), W610–W614.

Suhre, K., Sanejouand, Y. H. (2004). On the potential of normal-mode analysis for solving difficult molecular-replacement problems. *Acta Crystallog. D 60*, 796–799.